Electronic Supplementary Information

Reagent

Urea (≥99.0%, Sigma-Aldrich), melamine (≥99.0%, Sigma-Aldrich), potassium iodide (≥99.5%, Merck), potassium hydrogen phthalate (≥99.5%, Sigma-Aldrich), sodium hydroxide (≥97.0%, Merck), 5,5-dimethyl-1-pyrroline N-oxide, DMPO (≥99%, Sigma-Aldrich), 2,2,6,6-tetramethylpiperidine- 1-oxyl, TEMPO (99%, Sigma-Aldrich), 2,2,6,6-Tetramethylpiperidine, TEMP (≥99.0%, Sigma-Aldrich), 1,4-benzoquinone (≥98.0%, Sigma-Aldrich), silver nitrate (≥99.0%, Merck), *tert*-butanol (≥99.0%, Merck), anatase and rutile TiO_2 (99.5%, Sigma-Aldrich) were used as received. Ultrapure water procured from the Milli-Q® system was used throughout all the experiments.

Synthesis

To synthesize the triazine sample, 4.5 g of urea and then 0.5 g of melamine were placed in a combustion boat partially covered with aluminum foil and calcined in a tube furnace at 550 °C for 2 h with a heating rate of 10 °C min^{-1} under a mildly reducing atmosphere (5 vol% H_2 in N_2, 20 mL min^{-1}). After cooling to room temperature, the product was ground, washed with water until neutral pH was reached, and dried under vacuum at 80 °C for 12 h. For comparison, the heptazine sample was prepared using the same precursor composition but calcined in a crucible fully covered with aluminum foil at 550 °C for 2 h (10 °C min^{-1}) in a muffle furnace under air. The resulting product was treated identically by grinding, washing to neutral pH, and vacuum drying at 80 °C for 12 h.

Characterization

The microstructure was analyzed by XRD (Aeris Panalytical). Morphological characteristics were observed using SEM (Thermo Apreo 2) and TEM (Talos F200X). The specific surface area was determined using an adsorption analyzer (TriStar II 3020). O_2 adsorption on the photocatalysts was measured by TPD using a chemisorption analyzer (ChemiSorb 2750). Optical properties were evaluated by DRS using a UV–Vis–NIR spectrophotometer (Lambda 950). The chemical states of surface elements were analyzed by XPS (AXIS Supra+). TRMC measurements were conducted with the third harmonic of a Nd:YAG laser (Vibrant II, Opotek) for photoexcitation. PL spectra were produced from a fluorophotometer (Shimadzu, RF-5301PC).

Photocatalytic H_2O_2 production

For each experiment, 10 mg of photocatalyst powder was dispersed in 20 mL of deionized water (pH ~8) and subjected to ultrasonic treatment for 30 min to ensure complete dispersion. The suspension was then purged with O_2 in the dark for 1 h to achieve oxygen saturation. Photocatalytic reactions were initiated under continuous magnetic stirring by irradiating the suspension with a 90 W LED lamp emitting visible light ($\lambda > 390$ nm). During the reaction, air or O_2 was continuously supplied at a flow rate of 20 mL min^{-1}, and the temperature was maintained at 25 °C using a circulating water bath. The average light intensity was approximately 420 W m^{-2}. At determined intervals, 1 mL aliquots were withdrawn from the reaction mixture for quantifying the reaction product.

Determination of H_2O_2 concentration

The concentration of hydrogen peroxide produced during the photocatalytic reaction was determined using an iodometric spectrophotometric method.[1] In a typical analysis, 1.0 mL of the reaction supernatant was collected and mixed with 0.5 mL of 0.4 mol L^{-1} potassium iodide (KI) solution and 0.5 mL of 0.1 mol L^{-1} potassium hydrogen phthalate ($C_8H_5KO_4$) solution. Potassium

hydrogen phthalate provides a weakly acidic environment that facilitates the oxidation of iodide by hydrogen peroxide. The mixture was allowed to react in the dark for 30 min to ensure complete reaction. Under acidic conditions, hydrogen peroxide oxidizes iodide ions (I^-) to iodine (I_2), which subsequently reacts with excess iodide ions to form the triiodide ion (I_3^-). The reactions involved are expressed as:

$$H_2O_2 + 2I^- + 2H^+ \rightarrow I_2 + 2H_2O$$
$$I_2 + I^- \rightarrow I_3^-$$

The generated triiodide ion exhibits a characteristic absorption band at approximately 350 nm. The absorbance of the solution was measured using a UV–Vis spectrophotometer, and the concentration of H_2O_2 was determined from a calibration curve prepared using standard hydrogen peroxide solutions under identical conditions. All measurements were conducted at least three times to ensure reproducibility, and the average values were reported.

Determination of apparent quantum yield (AQY)

To determine the AQY value, photocatalytic reactions were carried out with 20 mg of photocatalyst powder dispersed in 20 mL of deionized water using a 300 W Xenon lamp equipped with a narrow bandpass filter to provide monochromatic illumination. The AQY was calculated using the following equation.

$$\text{AQY}\ (\%) = \left(\frac{2vN_Ahc}{IA\lambda}\right) \times 100$$

Where:

- v is the rate of BAL production (mol s^{-1})
- N_A is the Avogadro's number (6.02×10^{23} mol^{-1})
- h is Planck's constant (6.62×10^{-34} J s)
- c is the speed of light (3.0×10^8 m s^{-1})
- I is the light irradiance (760 W m^{-2})
- A is the irradiation area (2.83×10^{-5} m^2)
- λ is the light wavelength (360, 420, 450, 550, or 600 nm)

Determination of solar-to-chemical conversion (SCC) efficiency

To determine the SCC efficiency, photocatalytic reactions were performed with 50 mg of photocatalyst powder dispersed in 50 mL of deionized water using a 300 W Xenon lamp equipped with an AM 1.5G filter, delivering an incident light intensity of 1000 W m^{-2} (1 sun). The SCC was calculated using the following equation.

$$\text{SCC}\ (\%) = \frac{n \times \Delta G}{I \times A \times t} \times 100$$

Where:

- n is moles of H_2O_2 formed (mol)
- ΔG is Gibbs free energy change for H_2O_2 formation (117 kJ mol^{-1})
- I is the light irradiance (1000 W m^{-2})
- A is the irradiation area (2.83×10^{-5} m^2)
- t is irradiation time (s)

DFT calculation

All calculations were performed using ORCA version 6.1.1 with SHARK integral generation and digestion system.[2, 3] Initial molecular geometries were optimized using the Becke–Perdew 1986 (BP86) exchange-correlation functional in combination with the split-valence (SV) basis set, employing slow self-consistent field (SlowConv) convergence. Final geometry optimizations were carried out using the Becke, three-parameter, Lee–Yang–Parr (B3LYP) hybrid exchange–correlation functional together with the triple-zeta valence plus polarization (TZVP) basis set, employing no resolution-of-identity approximation (NoRI) and tight self-consistent field convergence criteria (TightSCF) to improve convergence reliability. All optimized structures correspond to fully converged minima at the B3LYP/TZVP level. Molecular structures were visualized using the program Chemcraft (version 1.8, build 682).

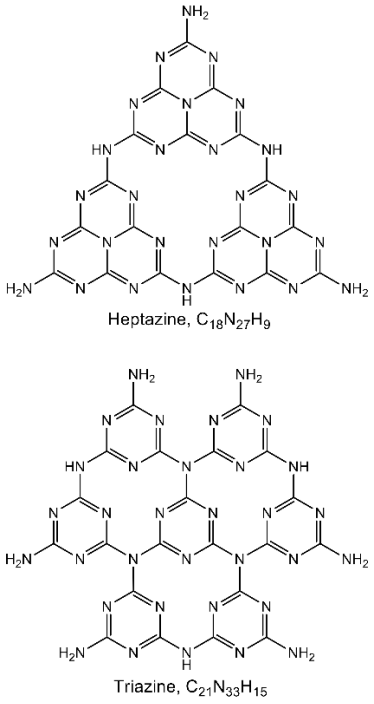

Figure S1. Molecular unit structures of heptazine and triazine in graphitic C_3N_4.

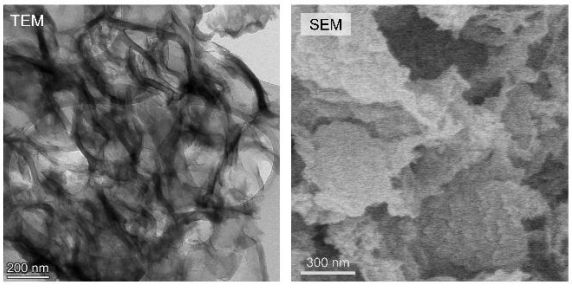

Figure S2. Electron micrographs of the heptazine sample.

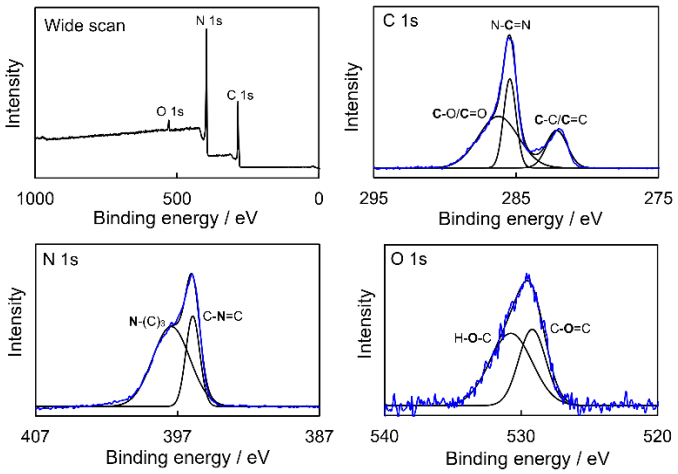

Figure S3. XPS spectra of the heptazine sample.

Table S1. Performance comparison of defective g-CN for photocatalytic H_2O_2 in pure water.

Catalyst	Notes	Light source	Catalyst weight / mg	H_2O_2 evolution rate / μM h^{-1}	Ref.
C_v-CN	C defects	λ > 420 nm	100	96	4
PuCN	Porous ultrathin; N defects	λ > 420 nm	30	41	1
N_v-CN	N defects	λ > 420 nm	50	76	5
R_{370}-CN	The reduction product of g-C_3N_4-450 at 370 °C using $NaBH_4$, N defects	λ > 420 nm	100	170	6
B_3CN	Calcination at a mass ratio of $NaBH_4$ to CN of 3; N defects and —C≡N	λ > 420 nm	10	114	7
V_s-CN	N defects and —C≡N	λ > 420 nm	30	85	8
U-CN	Ultra-thin CN prepared by exfoliation	λ > 400 nm	30	73	9
C_v-CN	C defects	λ > 390 nm	10	115	Present work
Anatase TiO_2	Commercial sample	λ > 390 nm	10	4	Present work
Rutile TiO_2	Commercial sample	λ > 390 nm	10	Not detected	Present work

References

1. X. Zhang, H. Su, P. Cui, Y. Cao, Z. Teng, Q. Zhang, Y. Wang, Y. Feng, R. Feng and J. Hou, *Nature Communications*, 2023, **14**, 7115.
2. F. Neese, *Wiley Interdisciplinary Reviews: Computational Molecular Science*, 2025, **15**, e70019.
3. F. Neese, *Journal of Computational Chemistry*, 2023, **44**, 381-396.
4. S. Li, G. Dong, R. Hailili, L. Yang, Y. Li, F. Wang, Y. Zeng and C. Wang, *Applied Catalysis B: Environmental*, 2016, **190**, 26-35.

5. Y. Lu, Y. Guo, S. Zhang, L. Li, R. Jiang, D. Zhang, J. C. Yu and J. Wang, *ACS nano*, 2024, **18**, 20435-20448.
6. Z. Zhu, H. Pan, M. Murugananthan, J. Gong and Y. Zhang, *Applied Catalysis B: Environmental*, 2018, **232**, 19-25.
7. B. Sheng, J. Li and J. Zhang, *Applied Catalysis A: General*, 2025, **701**, 120311.
8. W. Zeng, Y. Dong, X. Ye, Y. Zhao, Z. Zhang, T. Zhang, L. Zhang, J. Chen and X. Guan, *ACS Catalysis*, 2025, **15**, 6036-6045.
9. Y. Peng, H. Wang, R. Li, N. Teng, L. Ding, H. Wu, T. Sakurai, S. Liang, Y. Shimoyama and K. Sato, *Journal of Materials Chemistry A*, 2025, **13**, 37883-37896.